CANADIAN JOURNAL OF EXPLORATION GEOPHYSICS
VOL. 29, NO. 1 (JUNE 1993). P. 380-390

SHEAR-WAVE POLARIZATIONS AND POSSIBLE TEMPORAL VARIATIONS IN SHEAR-WAVE SPLITTING AT PARKFIELD

YUN LIU[1,2], DAVID C. BOOTH[1], STUART CRAMPIN[1,2], RUSS EVANS[1] AND PETER LEARY[3]

ABSTRACT

Five of the seven stations of the local borehole seismic network on the San Andreas Fault at Parkfield in central California exhibit aligned polarizations of first arriving split shear waves from fault zone earthquakes in an 18-month data set. At stations VC, VR and ED, 1 to 5 km from the fault, the polarizations are consistently normal or subnormal to the fault strike and parallel to the direction of maximum horizontal regional stress. Shear-wave first motion at station JN is 45°from the fault strike but may be influenced by local surface and subsurface topography. Station MM, located within or immediately adjacent to the fault zone, shows first motion polarized parallel to the fault strike. At stations VC and MM, the shear wave train signal-to-noise ratio permits positive identification and timing of the second split shear wave. There is some evidence of temporal variations of the shear-wave time delays in association with a M_L = 4 San Andreas fault earthquake, with the time delays at MM (7ms/km) twice those at VC (4ms/km). The relatively greater shear-wave splitting observed at MM suggests that the fluid-filled fractures within the fault zone are more extensive than in the surrounding crust. The fault-parallel polarization of the leading split shear wave at MM indicates that the stress is highly irregular in the immediate vicinity of the fault or that fault fractures tend to be aligned by fault shearing rather than by the regional principal stress.

INTRODUCTION

Shear-wave splitting is caused by the effective anisotropy of the medium in which the waves propagate. In the Earth's crust, the polarizations of the leading split shear waves typically display parallel alignments approximately orthogonal to the direction of minimum horizontal compressional stress (Crampin and Lovell, 1991). Splitting was first positively identified in the crust above small earthquakes in Turkey by Crampin et al. (1980, 1985) and has been subsequently observed in many parts of the world in a wide variety of rocks in a wide variety of tectonic regimes (reviewed by Crampin, 1987, and Crampin and Lovell, 1991). The splitting has been attributed to propagation through distributions of stress-aligned fluid-filled inclusions known as extensive-dilatancy anisotropy or EDA (Crampin and Lovell, 1991). It has been suggested that since such fluid-filled cracks, microcracks and preferentially oriented pore space are the most compliant elements of the rock mass, variations in the stress field may modify the EDA-crack geometry with consequent temporal changes in the orientation and degree of the shear-wave splitting (Crampin and Lovell, 1991). Variations of time delay between split shear waves are believed to have been observed at or near the time of the M_L = 6 1986 North Palm Springs earthquake (Peacock et al., 1988; Crampin et al., 1990) and an M_L = 3.5 earthquake of the 1982 Enola swarm in Arkansas (Booth et al., 1990). We have analyzed data recorded at the Parkfield network during a period of one and one half years to document shear-wave polarization alignments and to search for possible temporal variations in shear-wave splitting.

THE PARKFIELD HRSN NETWORK

It has been suggested that a magnitude M_L = 6 earthquake on the San Andreas fault could occur within the next few years at a nucleation zone near Middle Mountain (MM), Parkfield, California (Bakun and McEvilly, 1984; Bakun and Lindh, 1985). The Parkfield High Resolution Downhole Digital Seismic Network (HRSN), designed to monitor the characteristics of earthquakes before the anticipated event, was installed as part of the Parkfield Prediction Experiment (PPE). Both the uphole and downhole sensors of HRSN are typically three-component 2-Hz Mark Products L22E seismometers. The downhole seismometers are cemented at depths between 200 m and 300 m. They have a sampling rate of 500 Hz, a low-pass filter at 100 Hz and downhole gains of 60 dB. An accurate 3-D velocity model of the study region was an early result of the PPE research program (Michelini and McEvilly, 1991) and the details of the Parkfield network are documented by Blakeslee and Malin (1990).

'British Geological Survey, Murchison House, West Mains Road, Edinburgh EH9 3LA
*Department of Geology and Geophysics, University of Edinburgh, West Mains Road, Edinburgh EH9 3JW
[3]Department of Geological Science, University of Southern California, Los Angeles, CA 90089 - 074 1

We thank Prof. Tom McEvilly for his suggestions and discussion. We also thank Prof. Peter Malin for providing a further data set. This work is supported by the Natural Environment Research Council and is published with the approval of the Director of the British Geological Survey (NERC).

GEOLOGY

The geology of the Parkfieid area is dominated by the strike-slip plate boundary at the San Andreas Fault (SAF). Figure 1 shows the SAF and associated shallow thrust faults and the station distribution of the Parkfield HRSN network. The Parkfield fault segment is generally understood to be the transition zone between the 170-km-long creeping part of the SAF (average 33 mm/yr, Wesson et al., 1973) to the northwest and the 300-km-long locked portion to the southeast, where the average width of fault gouge in the Parkfield segment varies from 100 to 200 m. Analysis of seismograms recorded at MM in terms of fault zone trapped waves (Li and Leary, 1990; Leary and Ben-Zion, 1992) indicates that the shear-wave velocity of the fault gouge is about 1.1 km/s in the area of the 1966 M_L = 5.9 main shock and is 1.8 km/s in the southeast segment approaching the locked portion of the SAF. There exists a transition zone about 400 m wide with shear-wave velocity of 1.8 km/s on the flank of 1966 main shock area and 2.5 km/s on the northwest and southeast segment of the SAF. The fault is dipping steeply at 86" fl. 1" (Nishioka and Michael, 1990).

The Salinian block on the southwest side of the SAF consists of Gabilan plutonic and metamorphic basement rocks covered by a maximum of 2 km of Tertiary and Quaternary sediments. These deposits generally dip away from the Cholame Hills high, a basement uplift that parallels the SAF system several kilometres to its southwest. Northeast of the SAF, the broadly outcropping basement consists of Franciscan melange. Overlying this basement to the east are several kilometres of Cretaceous and younger sediments of the Great Valley sequence. In general, Franciscan rocks are moderately to strongly deformed and, in the SAF zone, slivers of various crystalline rocks appear to have been trapped within older branches of the fault (Brown et al., 1967). Some

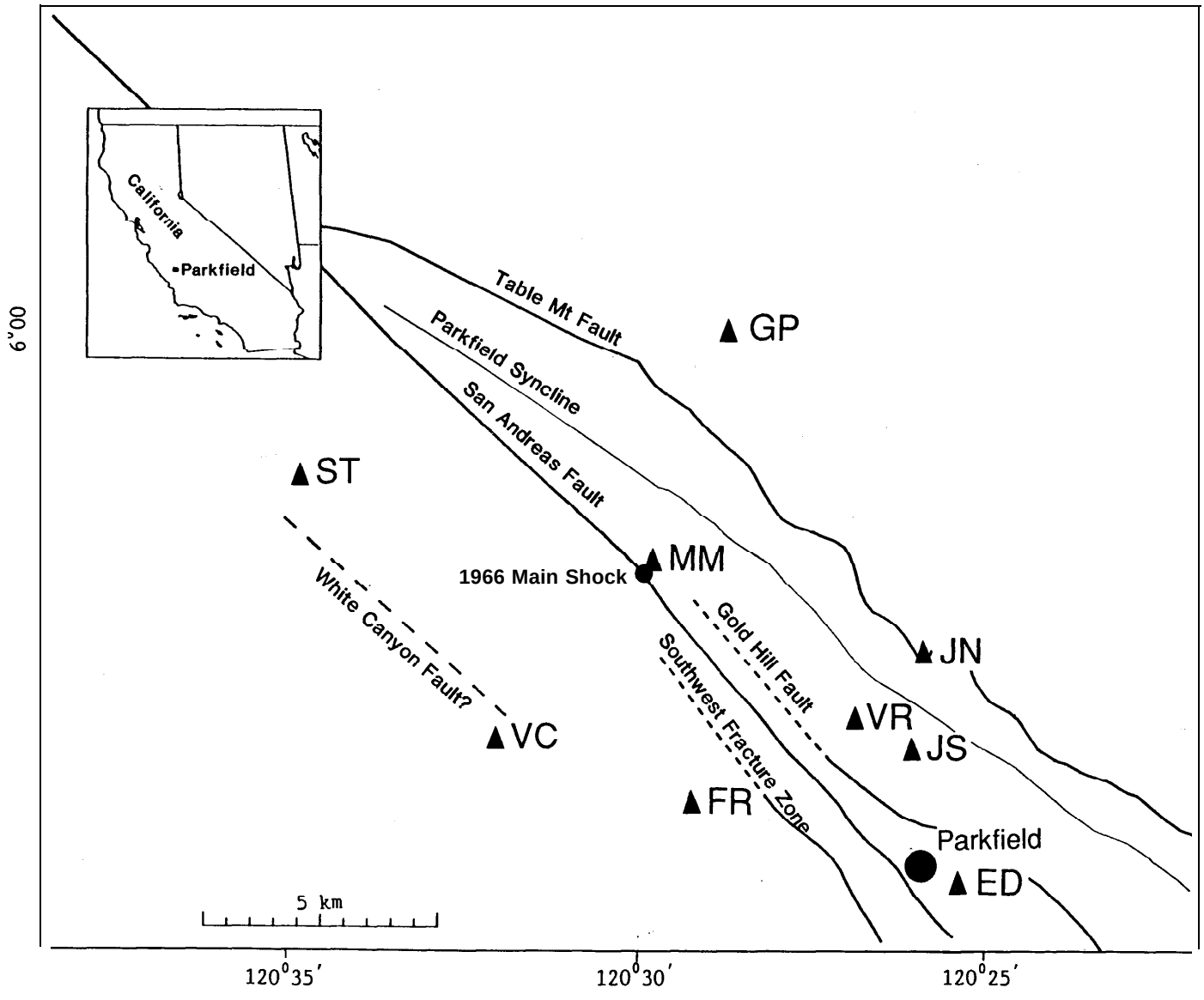

Fig. 1. Map of major faults and station distribution of the Parkfield downhole HRSN network. Triangles denote station locations.

of the numerous thrust faults surrounding the SAF show Holocene movement.

DATA ANALYSIS

Data recorded within the shear-wave windows (Evans, 1984; Booth and Crampin, 1985) of nine HRSN stations between January, 1989, and July, 1990, were examined. All earthquakes where shear waves were clearly visible above the P-wave coda showed evidence of shear-wave splitting. (The only earthquakes which did not show actual splitting were those where the source excited only one of the anisotropic shear-wave polarizations.) The epicentres of these local events within the shear-wave window of the Parkfield stations are shown in Figure 2. In general, earthquakes recorded by the network occur close to the fault plane with depths between 4 and 15 km and magnitudes between M_L = -0.5 and M_L = 2. An earthquake on 25th May, 1989, with

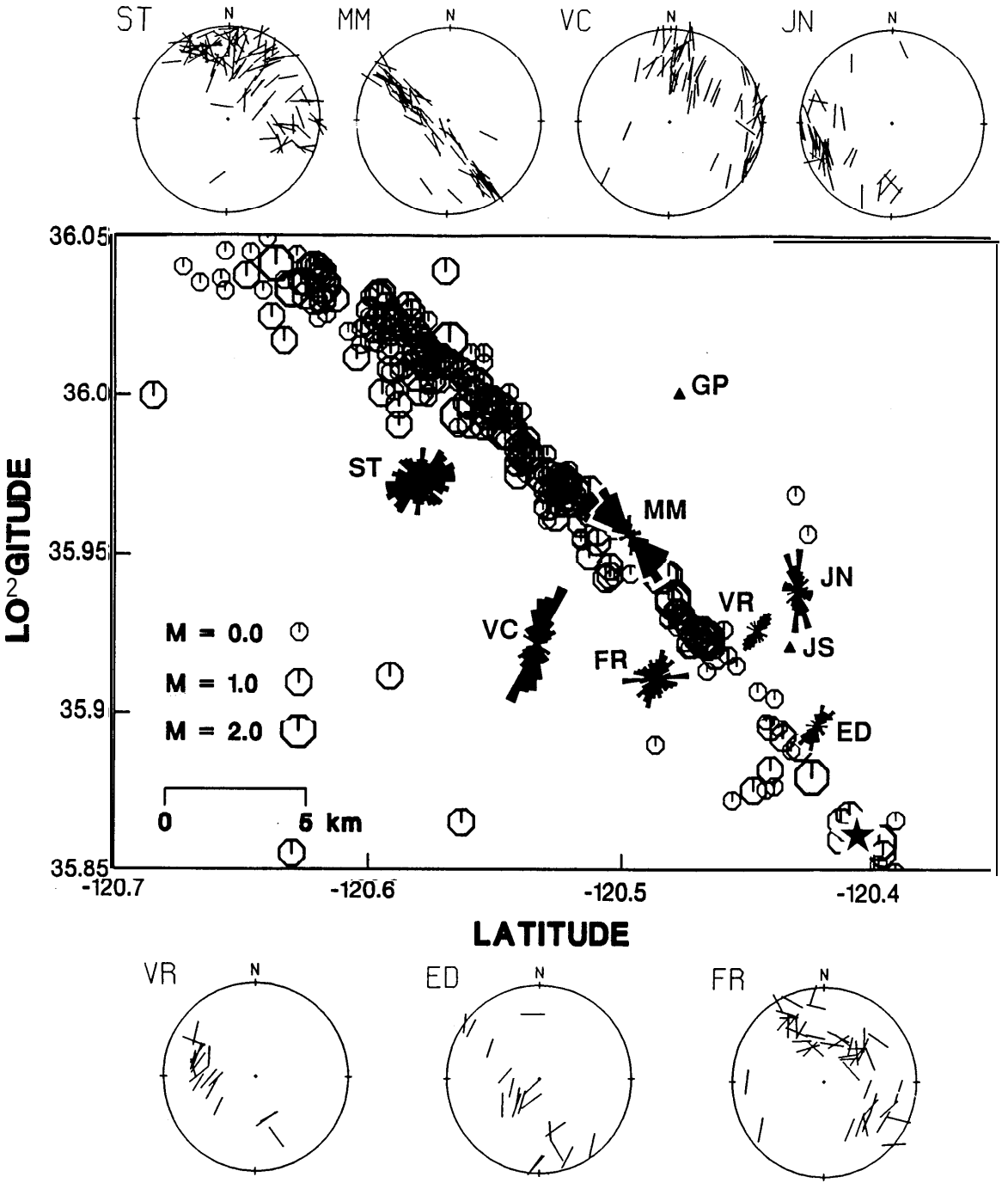

Fig. 2. Equal-area rose diagrams of polarizations of the leading split shear wave and the epicentres of the local events which are used to monitor the shear-wave splitting. The star indicates the M_L = 4 earthquake which occurred on May 25, 1989. Equal-area projections of the lower hemispheres beneath each station, out to angle of incidence of 45°, show polarizations of leading split shear waves. There are no suitable data at stations GP and JS.

magnitude M_L = 4 and focal depth of 8.25 km is located near the southeast extremity of the network and is marked with a star in Figure 2. It is about 15 km away from stations MM and VC. This is the largest earthquake which occurred on the 54-km Parkfield segment and its surrounding areas since the recording began, and we seek temporal variations associated with this event.

Representative records exhibiting clear shear-wave splitting are shown in Figure 3 with parameters listed in Table 1. Many seismograms are complicated with a strong P-wave coda which interferes with shear-wave arrivals particularly at stations ST and FR. This causes difficulty in identifying the onset of the faster split shear waves and we have not attempted to study the variation of time delays at these stations. Station GP is outside the shear-wave window for most earthquakes and those that are within the window have low-frequency shear waves (less than 10 Hz compared to the dominant frequency at about 20 Hz at other stations) yielding elliptical motion which makes analysis of shear-wave splitting difficult. The recording system at station JS did not function correctly during the period we are examining.

Ben-Zion and Malin (1991) and Ben-Zion et al. (1992) have identifed *P* head waves propagating along the fault plane at stations on the northeast side of the SAF (stations MM, JN, ED and VR). We would expect shear head waves to be observed in similar situations, where they might interfere with the split shear-wave arrivals. The characteristics of shear head waves along the fault plane have been examined with synthetic seismograms and will be the subject of a separate study. We find that shear head waves are probably not important for the study of shear-wave splitting as the amplitude of such shear head waves decays rapidly with the distance from the fault plane and the recorded energy at many of the HRSN stations is small. In any case, their characteristic one-sided waveforms are easily recognizable. We have attempted to eliminate both shear head waves and free surface S-P converted waves (the local *SP* phase) (Booth and Crampin, 1985; Crampin, 1990) from the data set in order to reduce the possibility of misidentifying the onset of the faster split shear waves.

Shear-wave polarizations

The distributions of shear-wave polarizations for shear-wave arrivals within the shear-wave window at each station are plotted as equal-area rose diagrams in Figure 2. The polarizations of the faster split shear waves display approximately parallel alignments at stations MM, VC, VR, JN and ED, as is typically observed elsewhere (Crampin and Lovell, 199 1). The directions of the polarizations are scattered at stations ST and FR with little evidence of any preferential alignment. The rose diagrams showing polarizations at stations VC, VR and ED are distributed about a N30°E direction which is approximately parallel to the direction of maximum principal stress near the San Andreas Fault in central California (Zoback et al., 1987). The alignment at JN is N5°W and the alignment at MM is about N40°W, approximately parallel to the SAF. [Note that VR shows a large scatter, similar to the scatter seen in the shear-wave VSP observations sampling the uppermost 1400 m of the Varian Well (VR) (Daley and McEvilly, 1990), although the average polarization in Figure 2 is clearly approximately N30°E.]

The reasons for the irregularities in the alignment of such shear-wave polarizations are not fully understood. Certainly, the interaction of shear waves with severe surface topography can in some cases cause parallel polarizations to be systematically rotated by up to 90" (Chen et al., 1987; Graham and Crampin, 1993) and hilltop sites typically display scattered polarizations (Peacock et al,, 1988). This sensitivity to topography within 100 m of the recording site is expected as shear waves have severe interactions with the free surface for angles of incidence outside the shear-wave window (Evans, 1984; Booth and Crampin, 1985). Focussing effects and changes in angle of incidence at the free surface due to refraction across near-surface high-impedance hard rock to sediment interfaces may also distort shear-wave arrivals (Crampin, 1990). Several of the HRSN stations (MM, ST, JN and GP) are sited near severe local topography and the subsurface structure beneath many of the stations is complicated.

Time delays between split shear waves

Time delays between the split shear waves are more difficult to estimate than polarizations of the faster split shear wave (Booth and Crampin, 1985; Chen et al., 1987), and scattered polarizations usually indicate other disturbances to the wave train which make it impossible to estimate reliably time delays. Consequently, we confine our analysis to those stations MM, VC, JN and ED, which display approximately parallel polarizations, excluding VR which has no data for the initial 8 months of the period we are examining.

Figure 4 shows the variations of time delay in polar projections of the shear-wave window for stations MM, VC, JN and ED and variations with time of the time delay, shear-wave polarization, and of the focal depths of the earthquakes whose records are analyzed. The time delays have been normalized to a path length of 1 km. The time of the M_L = 4 earthquake is indicated by the solid arrows in the time variations.

There is insufficient data to make reliable judgements of variations in time delay before the time of the M_L = 4 earthquake, but the stations where there is adequate data, MM and VC, show a (marginal) decrease in the time delay following the M_L = 4 earthquake, followed by an irregular increase. Note that the possible significance of this earthquake was not recognized initially and only came to our attention after we had observed the variation of time delays. There is no other larger earthquake recorded in the network during the study period. This behaviour is similar to that seen in previous studies which showed similar decreases in time delay at the time of M = 6 (Crampin et al., 1990) and M = 3.5 earthquakes (Booth et al., 1990).

The average time delays at station MM on the fault zone are about twice as large as those at station VC 5 km away from the fault zone on the southwest block. A large part of

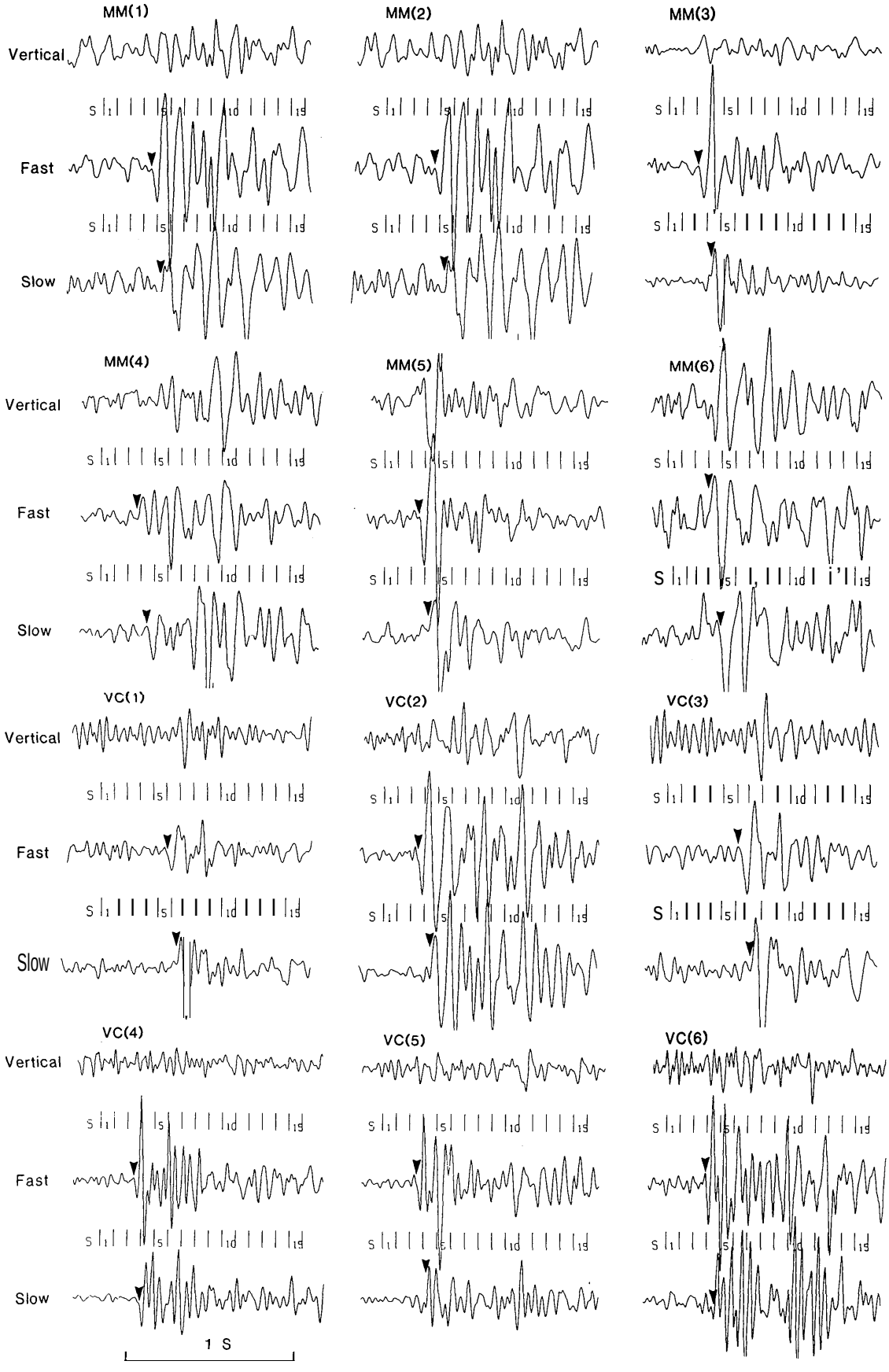

Fig. 3. Representative shear-wave seismograms and corresponding polarization diagrams recorded at stations MM and VC for events listed in Table 1. The horizontal components have been rotated parallel and perpendicular to the polarizations of the faster (F) and slower (S) split shear waves. The rotated seismograms show delayed shear-wave arrivals diagnostic of shear-wave splitting. The polarization diagrams show the horizontal particle motion for the numbered, 0.08-s-long, time windows marked on the seismograms.

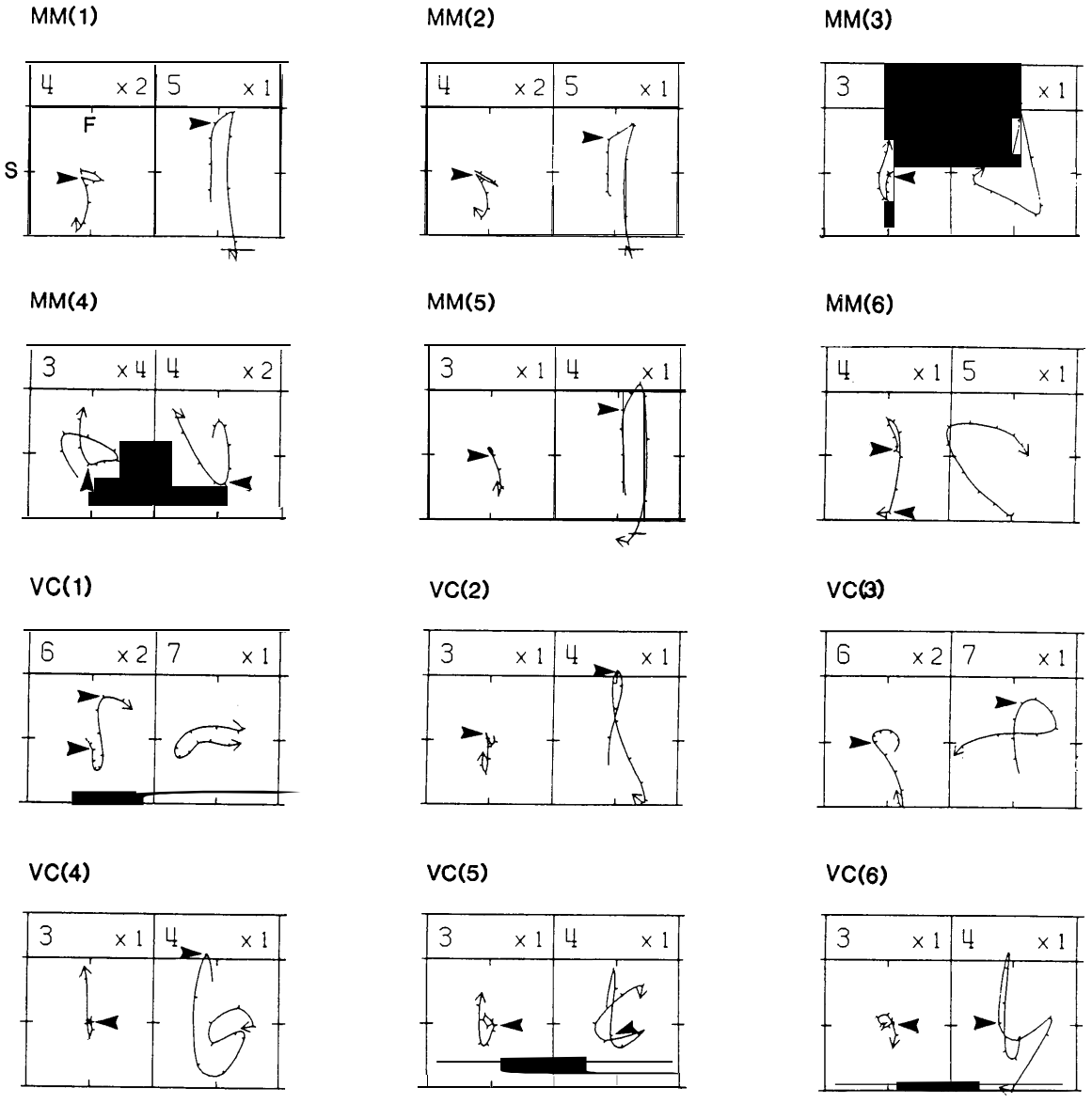

Fig. 3 (Cont'd).

Table 1. Parameters of representative earthquakes shown in Figure 2.

Stn(n)	Date (y.m.d)	Time (h.m)	Latitude (N)	Longitude (W)	Depth (km)	Mag. (M_L)	Spol (N°E)	Sdel (ms/km)
MM(1)	900613	2242	3555.51'	120°28.30'	5.80	1.05	328	**7.9**
MM(2)	900305	1632	35°57.47'	120°30.25'	4.47	-0.06	149	12.2
MM(3)	900614	1803	35'59.80'	120°33.65'	8.81	0.22	130	6.4
MM(4)	900505	2356	36°01.55'	120'35.01'	9.51	0.21	317	4.4
MM(5)	900613	2239	35°55.43'	120°28.18'	6.09	1.49	332	8.8
MM(6)	900405	0503	35°58.47'	120°31.53'	4.45	0.14	153	10.4
VC(1)	900511	1120	35°56.18'	120°28.94'	5.21	0.64	357	6.7
VC(2)	**900628**	**0249**	35°59.45'	120°35.38'	16.10	0.67	191	5.6
VC(3)	900511	1011	35°56.20'	120°28.89'	5.17	1.12	198	3.3
VC(4)	900702	2043	35°56.61'	120°30.39'	12.76	0.81	9	3.1
VC(5)	900516	1258	35°58.08'	120'31.49'	11.03	0.19	211	2.0
VC(6)	900412	0718	35'57.70'	120°31.65'	11.79	0.80	194	3.9

Stn(n):station name and numbercorrespondsto Figure 3. Spoland Sdelare shear-wave polarizations and time delays, respectively.

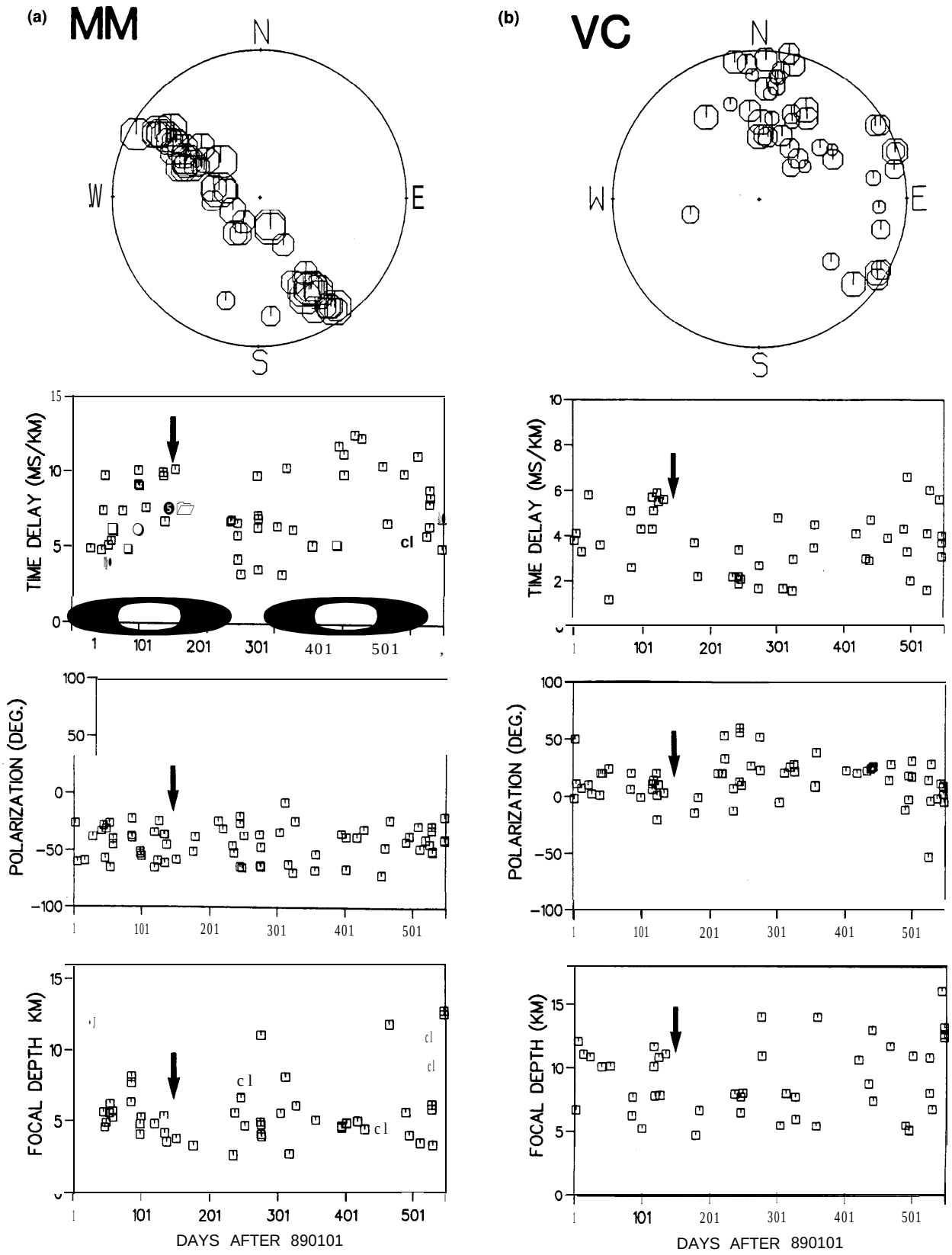

Fig. 4. Variations at stations: **(a)** MM; **(b)** VC; (c) JN and **(d)** ED. The diagrams show from the top: equal-area projections (polar maps) out to 45" of the time delays; variations of time delays with time from the beginning of the data set; variations of polarizations with time and (bottom) variations of focal depth with time. The arrows mark the time of the $M_L = 4$ earthquake.

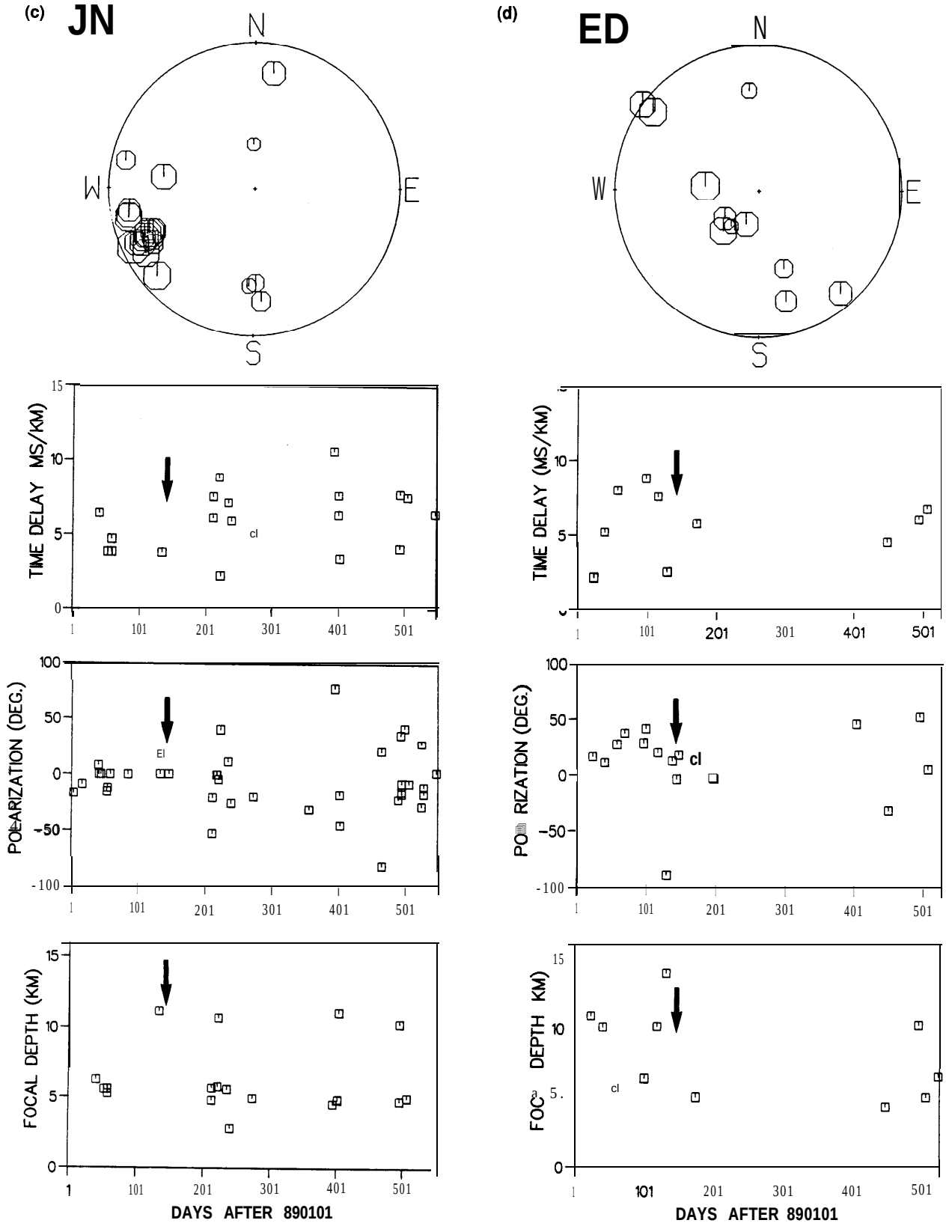
(c) JN
N
W
E
S
TIME DELAY MS/KM)
15
10
5
0
1
101
201
301
401
501
cl
POLARIZATION (DEG.)
100
50
0
-50
-100
El
FOCAL DEPTH (KM)
DAYS AFTER 890101
(d) ED
TIME DELAY (MS/KM)
POLARIZATION (DEG.)
cl
FOCAL DEPTH KM)
DAYS AFTER 890101

Fig. 4 (Cont'd).

each raypath to station MM is through the fault zone and the larger time delays are probably due to the greater density of microcracks and fractures trapped in the fault zone. The detailed geometry of these microcracks and fractures would be expected to be modified during any change in the stress field and could cause the possible temporal changes seen in Figure 4.

The corresponding polarizations show a relatively uniform scatter with no marked variation with time. The polarizations at stations MM and VC show a ±25° spread constant in time in a constant direction consistent with the rose diagrams in Figure 2. The polarizations at JN and ED show more scatter, again as expected from Figure 2. Note that the time delays at stations MM and VC are considered to be reliable, but at other stations the shear waves are severely distorted by strong *P* coda waves.

The variation of focal depth with time at stations MM and VC in the bottom diagram of Figure 4 shows a decrease in focal depth for about 100 days after the M_L = 4 event, which suggests that the decrease of time delay at the time of the event could be caused by migration of focal depths (note however the small numbers of earthquakes involved: 3 for MM and 7 for VC). Figure 5 shows the variation of the (normalized) time delay with the focal depth of the earthquakes monitored at each station in Figure 4. Stations VC (and ED) show a uniform scatter with no decrease of time delay with depth, as would be required if the anomalies in the temporal variations of time delay were caused by the decrease in focal depth indicated in Figure 4. However, for earthquakes near station MM (and JN), Figure 5 shows that at MM the normalised time delays have a pronounced increase for earthquakes with focal depths above about 7-km depth. This means that a decrease of focal depth, as observed in Figure 4, would tend to increase the time delays, and the temporal decrease is unlikely to be caused by depth migration.

The marked decrease in normalized time delays at MM for focal depths below 7 km suggests that the anisotropy of the fault zone is concentrated above 7 km. This could be explained by fault gouge having more aligned inclusions than the surrounding more intact rocks. The possible depth of the stronger anisotropy is in broad agreement with the results of Malin et al. (1989) and Li et al. (1992) who suggest that the fault gouge may extend from the surface to 10-km depth at the locked portion of the fault zone and about 5-km depth at the creeping portion. This intermediate depth of 7 km might suggest that MM is on a transition zone between creeping and locked sections of the fault.

DISCUSSION AND INTERPRETATION

Many studies have demonstrated that the alignment of shear-wave polarizations are not due to the source polarizations (Crampin et al., 1986; Peacock et al., 1988; Gledhill, 1990) and can be attributed to the effective anisotropy of stress-aligned fluid-filled inclusions (Crampin and Lovell, 1991). Shear-wave polarizations appear in most cases to be aligned parallel to the direction of the local maximum

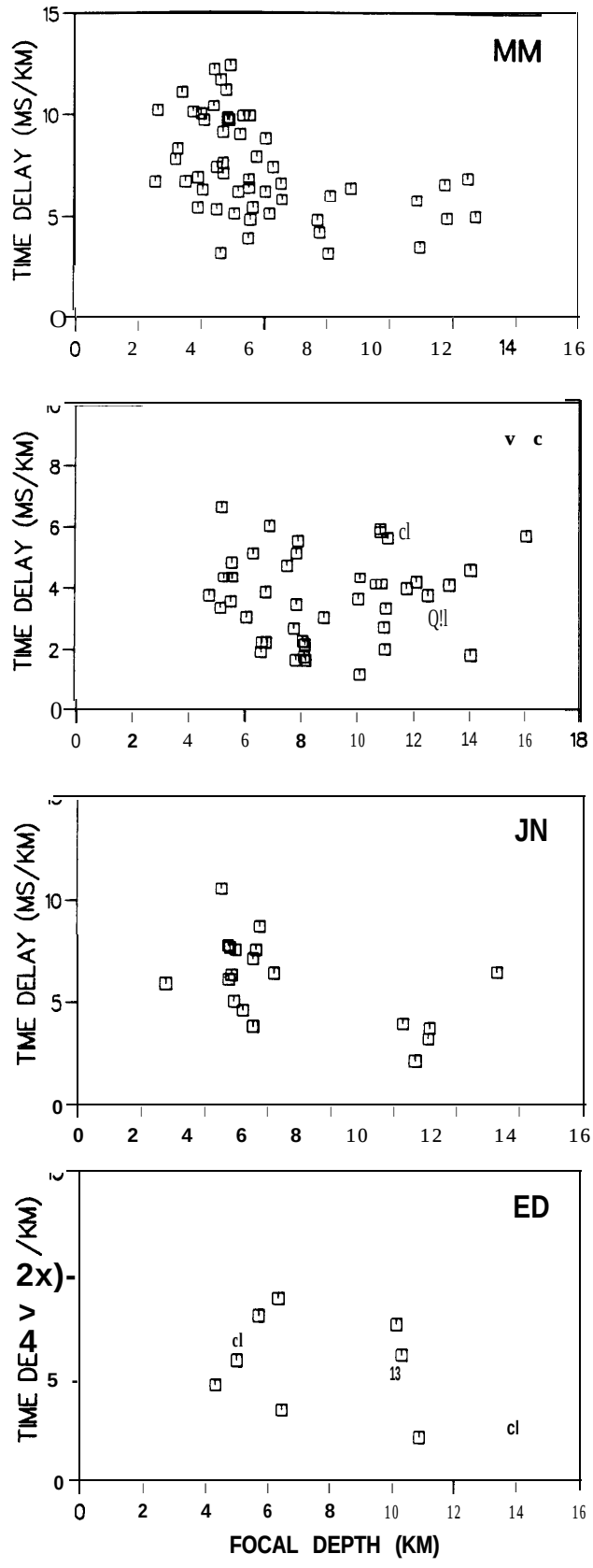

Fig. 5. Variations of (normalized) time delays with focal depth of the earthquakes monitored in Figure 4 .

compressional stress or, more strictly, perpendicular to the minimum stress direction which is expected to control the orientations of fluid-filled inclusions in the crust (Crampin and Lovell, 1991). Note that such parallelism constrains the type of anisotropic symmetry to hexagonal symmetry with a subhorizontal axis of symmetry. This strongly suggests a distribution of subparallel vertical EDA cracks as the source of the anisotropy since such structures are the only common source of hexagonal symmetry found in the crust (Crampin, 1993). The polarizations at VC, VR and ED in Figure 2 are approximately perpendicular to the SAF and parallel to the regional stress direction estimated by Zoback et al. (1987) and thus agree with the hypothesis of fluid-filled EDA cracks, in this case, aligned by the regional stress field.

Nearer the fault, the alignment of EDA cracks appears to change. Figure 6 plots the nodal lines of 68 fault plane solutions of earthquakes which were located close to station MM (Nishioka and Michael, 1990). The narrow distribution of inferred stress axes suggests a uniform stress field in the vicinity of the fault. However, the N15°W to N10°E direction of maximum principal stress implied by these mechanisms is not compatible with the N30°E microcrack direction inferred from shear-wave polarizations at VC, VR and ED, which are parallel to the regional principal stress. It is compatible with polarizations at JN but JN is in a region of high topographic relief.

If we accept the hypothesis of shear-wave splitting caused by aligned fluid-filled EDA cracks, the polarizations at MM suggest that the cracks strike parallel to the fault. Studies of shear fracture failure suggest the development of fault parallel fractures (King, 1983), while observations of shear waves specifically associated with fault zones at Izmit, Turkey (Crampin et al., 1985), Oroville, California (Lear-y et al., 1987) and at seismic station KNW on the San Jacinto Fault, California (Crampin et al., 1990) indicate the same conclusion.

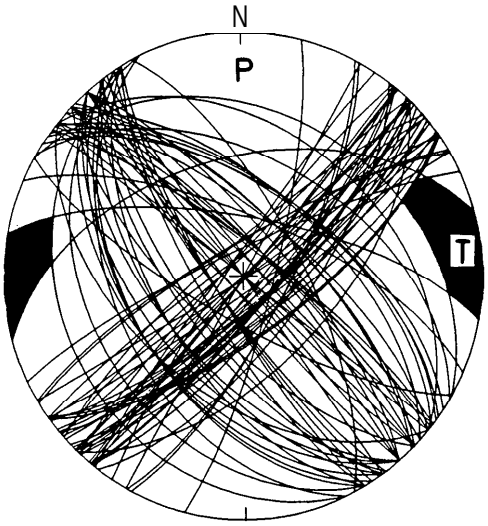

Fig. 6. Superimposed fault plane solutions from the Parkfield area showing common areas of compression (P) and tension (T), in equal-area projections of the upper focal hemisphere (after Nishioka and Michael, 1990).

Station MM is probably on the transition zone of the SAF and it is very close to the 1966 main shock (Figure 1). Ninety-five percent of shear waves from earthquakes recorded within the shear-wave window at this station propagated nearly vertically with an incidence angle of less than 15°, hence the fault internal structure (fault gouge and transition zone), its nearby subparallel folds and various crystalline rocks are presumably the dominant factors in controlling the shear-wave polarizations beneath this station. It is likely that the gouge of the fault zone plays the most significant role in controlling shear-wave anisotropy at this station.

The geological structure at Parkfield is complicated. The fault zone area appears to be heterogeneous in both velocity variation and geological structure (Michelini and McEvilly, 1991; Li et al., 1992). This is presumably one of the reasons for the difficulty in picking faster shear-wave onsets. Nevertheless, the results of this study correlate with other independent studies and we believe that the temporal variation of time delays is reliably associated with the $M_L = 4$ event.

CONCLUSIONS

The shear-wave polarizations at stations VC, ED and VR are aligned approximately NNE which is approximately parallel to the direction of maximum horizontal regional stress. Shear-wave first motion at station JN is 45" from the fault strike but may be influenced by local surface and subsurface topography. Polarizations at station MM are probably controlled by the fault zone internal structure causing an alignment of about N40°W parallel to the fault. The fact that time delays at station MM are about twice as large as those at VC suggests that the fluid-filled microcracks and fractures within the fault zone are more extensive than in the surrounding crust. Possible temporal changes in the time delays between split shear waves have been observed at two stations of the Parkfield HRSN network after an $M_L = 4$ earthquake with epicentre about 15 km from the stations. The temporal changes suggested in this paper are compatible with similar temporal variations at the time of a larger earthquake observed elsewhere.

REFERENCES

Bakun, W.H. and Lindh, A.G., 1985, The Parkfield, California, earthquake prediction experiment: Science **229**, 6 19-623.

_____ and McEvilly, T.V., 1984, Recurrence models and Parkfield, California, earthquakes: J. Geophys. Res. 89,305 l-3058.

Ben-Zion, Y. and Malin, P., 1991, San Andreas fault zone head waves near Parkfield, California: Science 251, 1592- 1594.

_____, Katz, S. and Leary, P., 1992, Joint inversion of fault zone head waves and direct *P* arrivals for crustal structure near major faults: J. Geophys. Res. 97, 1943-1951.

Blakeslee, S.N. and Malin, P.E., 1990, A comparison of earthquake coda waves at surface versus subsurface seismometer: J. Geophys. Res. 95, 309-326.

Booth, D.C. and Crampin, S., 1985, Shear-wave polarizations on a curved wavefront at an isotropic free surface: Geophys. J. Roy. Astr. Soc., **83**, 3 l-45.

_____, _____, Lovell, J.H. and Chiu, J.-M., 1990, Temporal changes in shear-wave splitting during an earthquake swarm in Arkansas: J. Geophys. Res. 95, 11,151-l 1,164.

Brown, R.D., Jr., Vedder, J.G., Wallace, R.E., Roth, E.F., Yerkes, R.F., Castle, R.O., Waananen, A.O., Page, R.W. and Eaton, J.P., 1967, The Parkfield-Cholame, California earthquakes of June-August 1966 - surface geologic effects, water-resources aspects and preliminary seismic data: U.S. Geol. Surv., Prof. Paper 579, l-66.

Chen, T.-C., Booth, D.C. and Crampin, S., 1987, Shear-wave polarizations near the North Anatolian Fault - III. Observations of temporal changes: Geophys. J. Roy. Astr. Soc. **91**, 287-311.

Crampin, S., 1987, Geological and industrial implications of extensive-dilatancy anisotropy: Nature **328**, 49 l-496.

_____, 1990, The scattering of shear waves in the crust: Pure Appl. Geophys. **132**, 67-91.

_____, 1993, Arguments for EDA: Can. J. Expl. Geophys. 29, 18-30.

_____ and Booth, D.C., 1985, Shear-wave polarizations near the North Anatolian Fault – II. Interpretation in terms of crack-induced anisotropy: Geophys. J. Roy. Astr. Soc. **83**, 75-92.

_____ and Lovell, J.H., 1991, A decade of shear-wave splitting in the Earth's crust: what does it mean? what use can we make of it? and what should we do next?: Geophys. J. Intemat. **107**, 387-407.

, Booth, D.C., Evans, R., Peacock, S. and Fletcher, J.B., 1990, Changes in shear-wave splitting at Anza near the time of the North Palm Springs earthquake: J. Geophys. Res. 95, 11,197-l 1,212.

_____, _____, Krasnova, M.A., Chesnokov, E.M., Maximov, A.B. and Tarasov, N.T., 1986, Shear-wave polarizations in the Peter the First Range indicating crack-induced anisotropy in a thrust-fault regime: Geophys. J. Roy. Astr. Soc. **84**, 401-412.

- 9 Evans, R. and Üçer, S.B., 1985, Analysis of records of local earthquakes: the Turkish Dilatancy Projects (TDP1 and TDP2): Geophys, J. Roy. Astr. Soc. 83, 1- 16.

_____, _____, _____, Doyle, M., Davis, J.P., Yegorkina, G.V. and Miller, A., 1980, Observations of dilatancy-induced polarization anomalies and earthquake prediction: Nature 2, 874-877.

Daley, T.M. and McEvilly, T.V., 1990, Shear-wave anisotropy in the Parkfield Varian Well VSP: Bull. Seis. Soc. Am. **80**, 857-869.

Evans, R., 1984, Effects of the free surface on shear wavetrains: Geophys. J. Roy. Astr. Soc. 76, 165-172.

Gledhill, K.R., 1990, A shear-wave polarization study in the Wellington region, New Zealand: Geophys. Res. Lett. 17, 1319- 1322.

Graham, G. and Crampin, S., 1993, Shear-wave splitting from regional earthquakes in Turkey: Can. J. Expl. Geophys. 29, 37 l-379.

King, G.C.P., 1983, The accommodation of large fault behaviour, subsurface geology, and three-dimensional velocity models: Science 253, 651-654.

Leary, P.C. and Ben-Zion, Y., 1992, A 200-m-wide fault low-velocity layer on the San Andreas fault at Parkfield: results from analytic waveform fits to trapped wave groups: J. Geophys. Res. 97, 1943-1951.

_____, Li, Y.-G. and Aki, K., 1987, Observation and modelling of fault zone fracture seismic anisotropy – I. *P*, *SV* and *SH* traveltimes: Geophys. J. Roy. Astr. Soc. **91**, 461-484.

Li, Y.-G. and Leary, P.C., 1990, Fault zone trapped seismic waves: Bull. Seis. Soc. Am. **80**, 1245-127 1.

, Teng, T.L. and Aki, K., 1992, Observation and interpretation of fault-zone trapped seismic waves at three different geological and experiment environments in California: Seis. Res. Lett. **63**, 76 (Abstr.).

Malin, P.E., Blakeslee, S.N., Alvarez, M.G. and Martin, A.J., 1989, Microearthquake imaging of the Parkfield asperity: Science **224**, 557-559.

Michelini, A. and McEvilly, T.V., 199 1, Seismological studies at Parkfield – I. Simultaneous inversion for velocity structure and hypocenters using cubic B-splines parameterization: Bull. Seis. Soc. Am. **81**, 524-552.

Nishioka, G.K. and Michael, A.J., 1990, A detailed study of the seismicity of the Middle Mountain zone at Parkfield, California: Bull. Seis. Soc. Am, **80**, 577-588.

Peacock, S., Crampin, S., Booth, D.C. and Fletcher, J.B., 1988, Shear-wave splitting in the Anza seismic gap, southern California: temporal variations as possible precursors: J. Geophys. Res. 193, 3339-3356.

Wesson, R.L., Burford, R.O. and Ellsworth, W.L., 1973, Relationship between seismicity, fault creep and crustal loading along the central San Andreas fault: Stanford Univ. Publ. Geol. Sci. **13**, 303-321.

Zoback, M.D. et al., 1987, New evidence on the state of stress of the San Andreas Fault System: Science 238, 1105- 1111.